# Study of the decays $D^+ \to \eta^{(\prime)} e^+ \nu_e$

M. Ablikim,[1] M. N. Achasov,[9,d] S. Ahmed,[14] M. Albrecht,[4] A. Amoroso,[53a,53c] F. F. An,[1] Q. An,[50,40] Y. Bai,[39] O. Bakina,[24] R. Baldini Ferroli,[20a] Y. Ban,[32] D. W. Bennett,[19] J. V. Bennett,[5] N. Berger,[23] M. Bertani,[20a] D. Bettoni,[21a] J. M. Bian,[47] F. Bianchi,[53a,53c] E. Boger,[24,b] I. Boyko,[24] R. A. Briere,[5] H. Cai,[55] X. Cai,[1,40] O. Cakir,[43a] A. Calcaterra,[20a] G. F. Cao,[1,44] S. A. Cetin,[43b] J. Chai,[53c] J. F. Chang,[1,40] G. Chelkov,[24,b,c] G. Chen,[1] H. S. Chen,[1,44] J. C. Chen,[1] M. L. Chen,[1,40] P. L. Chen,[51] S. J. Chen,[30] X. R. Chen,[27] Y. B. Chen,[1,40] X. K. Chu,[32] G. Cibinetto,[21a] H. L. Dai,[1,40] J. P. Dai,[35,h] A. Dbeyssi,[14] D. Dedovich,[24] Z. Y. Deng,[1] A. Denig,[23] I. Denysenko,[24] M. Destefanis,[53a,53c] F. De Mori,[53a,53c] Y. Ding,[28] C. Dong,[31] J. Dong,[1,40] L. Y. Dong,[1,44] M. Y. Dong,[1,40,44] Z. L. Dou,[30] S. X. Du,[57] P. F. Duan,[1] J. Fang,[1,40] S. S. Fang,[1,44] X. Fang,[50,40] Y. Fang,[1] R. Farinelli,[21a,21b] L. Fava,[53b,53c] S. Fegan,[23] F. Feldbauer,[23] G. Felici,[20a] C. Q. Feng,[50,40] E. Fioravanti,[21a] M. Fritsch,[23,14] C. D. Fu,[1] Q. Gao,[1] X. L. Gao,[50,40] Y. Gao,[42] Y. G. Gao,[6] Z. Gao,[50,40] I. Garzia,[21a] K. Goetzen,[10] L. Gong,[31] W. X. Gong,[1,40] W. Gradl,[23] M. Greco,[53a,53c] M. H. Gu,[1,40] S. Gu,[15] Y. T. Gu,[12] A. Q. Guo,[1] L. B. Guo,[29] R. P. Guo,[1,44] Y. P. Guo,[23] Z. Haddadi,[26] S. Han,[55] X. Q. Hao,[15] F. A. Harris,[45] K. L. He,[1,44] X. Q. He,[49] F. H. Heinsius,[4] T. Held,[4] Y. K. Heng,[1,40,44] T. Holtmann,[4] Z. L. Hou,[1] C. Hu,[29] H. M. Hu,[1,44] T. Hu,[1,40,44] Y. Hu,[1] G. S. Huang,[50,40] J. S. Huang,[15] X. T. Huang,[34] X. Z. Huang,[30] Z. L. Huang,[28] T. Hussain,[52] W. Ikegami Andersson,[54] Q. Ji,[1] Q. P. Ji,[15] X. B. Ji,[1,44] X. L. Ji,[1,40] X. S. Jiang,[1,40,44] X. Y. Jiang,[31] J. B. Jiao,[34] Z. Jiao,[17] D. P. Jin,[1,40,44] S. Jin,[1,44] Y. Jin,[46] T. Johansson,[54] A. Julin,[47] N. Kalantar-Nayestanaki,[26] X. L. Kang,[1] X. S. Kang,[31] M. Kavatsyuk,[26] B. C. Ke,[5] T. Khan,[50,40] A. Khoukaz,[48] P. Kiese,[23] R. Kliemt,[10] L. Koch,[25] O. B. Kolcu,[43b,f] B. Kopf,[4] M. Kornicer,[45] M. Kuemmel,[4] M. Kuessner,[4] M. Kuhlmann,[4] A. Kupsc,[54] W. Kühn,[25] J. S. Lange,[25] M. Lara,[19] P. Larin,[14] L. Lavezzi,[53c] S. Leiber,[4] H. Leithoff,[23] C. Leng,[53c] C. Li,[54] Cheng Li,[50,40] D. M. Li,[57] F. Li,[1,40] F. Y. Li,[32] G. Li,[1] H. B. Li,[1,44] H. J. Li,[1,44] J. C. Li,[1] K. J. Li,[41] Kang Li,[13] Ke Li,[34] Lei Li,[3] P. L. Li,[50,40] P. R. Li,[44,7] Q. Y. Li,[34] T. Li,[34] W. D. Li,[1,44] W. G. Li,[1] X. L. Li,[34] X. N. Li,[1,40] X. Q. Li,[31] Z. B. Li,[41] H. Liang,[50,40] Y. F. Liang,[37] Y. T. Liang,[25] G. R. Liao,[11] D. X. Lin,[14] B. Liu,[35,h] B. J. Liu,[1] C. X. Liu,[1] D. Liu,[50,40] F. H. Liu,[36] Fang Liu,[1] Feng Liu,[6] H. B. Liu,[12] H. M. Liu,[1,44] Huanhuan Liu,[1] Huihui Liu,[16] J. B. Liu,[50,40] J. P. Liu,[55] J. Y. Liu,[1,44] K. Liu,[42] K. Y. Liu,[28] Ke Liu,[6] L. D. Liu,[32] P. L. Liu,[1,40] Q. Liu,[44] S. B. Liu,[50,40] X. Liu,[27] Y. B. Liu,[31] Z. A. Liu,[1,40,44] Zhiqing Liu,[23] Y. F. Long,[32] X. C. Lou,[1,40,44] H. J. Lu,[17] J. G. Lu,[1,40] Y. Lu,[1] Y. P. Lu,[1,40] C. L. Luo,[29] M. X. Luo,[56] X. L. Luo,[1,40] X. R. Lyu,[44] F. C. Ma,[28] H. L. Ma,[1] L. L. Ma,[34] M. M. Ma,[1,44] Q. M. Ma,[1] T. Ma,[1] X. N. Ma,[31] X. Y. Ma,[1,40] Y. M. Ma,[34] F. E. Maas,[14] M. Maggiora,[53a,53c] Q. A. Malik,[52] Y. J. Mao,[32] Z. P. Mao,[1] S. Marcello,[53a,53c] Z. X. Meng,[46] J. G. Messchendorp,[26] G. Mezzadri,[21a] J. Min,[1,40] T. J. Min,[1] R. E. Mitchell,[19] X. H. Mo,[1,40,44] Y. J. Mo,[6] C. Morales Morales,[14] G. Morello,[20a] N. Yu. Muchnoi,[9,d] H. Muramatsu,[47] A. Mustafa,[4] Y. Nefedov,[24] F. Nerling,[10] I. B. Nikolaev,[9,d] Z. Ning,[1,40] S. Nisar,[8] S. L. Niu,[1,40] X. Y. Niu,[1,44] S. L. Olsen,[33,j] Q. Ouyang,[1,40,44] S. Pacetti,[20b] Y. Pan,[50,40] M. Papenbrock,[54] P. Patteri,[20a] M. Pelizaeus,[4] J. Pellegrino,[53a,53c] H. P. Peng,[50,40] K. Peters,[10,g] J. Pettersson,[54] J. L. Ping,[29] R. G. Ping,[1,44] A. Pitka,[23] R. Poling,[47] V. Prasad,[50,40] H. R. Qi,[2] M. Qi,[30] S. Qian,[1,40] C. F. Qiao,[44] N. Qin,[55] X. S. Qin,[4] Z. H. Qin,[1,40] J. F. Qiu,[1] K. H. Rashid,[52,i] C. F. Redmer,[23] M. Richter,[4] M. Ripka,[23] M. Rolo,[53c] G. Rong,[1,44] Ch. Rosner,[14] X. D. Ruan,[12] A. Sarantsev,[24,e] M. Savrié,[21b] C. Schnier,[4] K. Schoenning,[54] W. Shan,[32] M. Shao,[50,40] C. P. Shen,[2] P. X. Shen,[31] X. Y. Shen,[1,44] H. Y. Sheng,[1] J. J. Song,[34] W. M. Song,[34] X. Y. Song,[1] S. Sosio,[53a,53c] C. Sowa,[4] S. Spataro,[53a,53c] G. X. Sun,[1] J. F. Sun,[15] L. Sun,[55] S. S. Sun,[1,44] X. H. Sun,[1] Y. J. Sun,[50,40] Y. K. Sun,[50,40] Y. Z. Sun,[1] Z. J. Sun,[1,40] Z. T. Sun,[19] C. J. Tang,[37] G. Y. Tang,[1] X. Tang,[1] I. Tapan,[43c] M. Tiemens,[26] B. Tsednee,[22] I. Uman,[43d] G. S. Varner,[45] B. Wang,[1] B. L. Wang,[44] D. Wang,[32] D. Y. Wang,[32] Dan Wang,[44] K. Wang,[1,40] L. L. Wang,[1] L. S. Wang,[1] M. Wang,[34] Meng Wang,[1,44] P. Wang,[1] P. L. Wang,[1] W. P. Wang,[50,40] X. F. Wang,[42] Y. Wang,[38] Y. D. Wang,[14] Y. F. Wang,[1,40,44] Y. Q. Wang,[23] Z. Wang,[1,40] Z. G. Wang,[1,40] Z. H. Wang,[50,40] Z. Y. Wang,[1] Zongyuan Wang,[1,44] T. Weber,[23] D. H. Wei,[11] P. Weidenkaff,[23] S. P. Wen,[1] U. Wiedner,[4] M. Wolke,[54] L. H. Wu,[1] L. J. Wu,[1,44] Z. Wu,[1,40] L. Xia,[50,40] X. Xia,[34] Y. Xia,[18] D. Xiao,[1] H. Xiao,[51] Y. J. Xiao,[1,44] Z. J. Xiao,[29] Y. G. Xie,[1,40] Y. H. Xie,[6] X. A. Xiong,[1,44] Q. L. Xiu,[1,40] G. F. Xu,[1] J. J. Xu,[1,44] L. Xu,[1] Q. J. Xu,[13] Q. N. Xu,[44] X. P. Xu,[38] L. Yan,[53a,53c] W. B. Yan,[50,40] W. C. Yan,[2] W. C. Yan,[50,40] Y. H. Yan,[18] H. J. Yang,[35,h] H. X. Yang,[1] L. Yang,[55] Y. H. Yang,[30] Y. X. Yang,[11] Yifan Yang,[1,44] M. Ye,[1,40] M. H. Ye,[7] J. H. Yin,[1] Z. Y. You,[41] B. X. Yu,[1,40,44] C. X. Yu,[31] J. S. Yu,[27] C. Z. Yuan,[1,44] Y. Yuan,[1] A. Yuncu,[43b,a] A. A. Zafar,[52] A. Zallo,[20a] Y. Zeng,[18] Z. Zeng,[50,40] B. X. Zhang,[1] B. Y. Zhang,[1,40] C. C. Zhang,[1] D. H. Zhang,[1] H. H. Zhang,[41] H. Y. Zhang,[1,40] J. Zhang,[1,44] J. L. Zhang,[1] J. Q. Zhang,[1] J. W. Zhang,[1,40,44] J. Y. Zhang,[1] J. Z. Zhang,[1,44] K. Zhang,[1,44] L. Zhang,[42] S. Q. Zhang,[31] X. Y. Zhang,[34] Y. H. Zhang,[1,40] Y. T. Zhang,[50,40] Yang Zhang,[1] Yao Zhang,[1] Yu Zhang,[44] Z. H. Zhang,[6] Z. P. Zhang,[50] Z. Y. Zhang,[55] G. Zhao,[1] J. W. Zhao,[1,40] J. Y. Zhao,[1,44] J. Z. Zhao,[1,40] Lei Zhao,[50,40] Ling Zhao,[1] M. G. Zhao,[31] Q. Zhao,[1] S. J. Zhao,[57] T. C. Zhao,[1] Y. B. Zhao,[1,40] Z. G. Zhao,[50,40] A. Zhemchugov,[24,b] B. Zheng,[51] J. P. Zheng,[1,40] W. J. Zheng,[34] Y. H. Zheng,[44] B. Zhong,[29] L. Zhou,[1,40] X. Zhou,[55] X. K. Zhou,[50,40] X. R. Zhou,[50,40] X. Y. Zhou,[1] Y. X. Zhou,[12] J. Zhu,[31] J. Zhu,[41] K. Zhu,[1] K. J. Zhu,[1,40,44] S. Zhu,[1] S. H. Zhu,[49] X. L. Zhu,[42] Y. C. Zhu,[50,40] Y. S. Zhu,[1,44] Z. A. Zhu,[1,44] J. Zhuang,[1,40] B. S. Zou,[1] and J. H. Zou[1]

 

(BESIII Collaboration)

[1]Institute of High Energy Physics, Beijing 100049, People's Republic of China
[2]Beihang University, Beijing 100191, People's Republic of China
[3]Beijing Institute of Petrochemical Technology, Beijing 102617, People's Republic of China
[4]Bochum Ruhr-University, D-44780 Bochum, Germany
[5]Carnegie Mellon University, Pittsburgh, Pennsylvania 15213, USA
[6]Central China Normal University, Wuhan 430079, People's Republic of China
[7]China Center of Advanced Science and Technology, Beijing 100190, People's Republic of China
[8]COMSATS Institute of Information Technology,
Lahore, Defence Road, Off Raiwind Road, 54000 Lahore, Pakistan
[9]G.I. Budker Institute of Nuclear Physics SB RAS (BINP), Novosibirsk 630090, Russia
[10]GSI Helmholtzcentre for Heavy Ion Research GmbH, D-64291 Darmstadt, Germany
[11]Guangxi Normal University, Guilin 541004, People's Republic of China
[12]Guangxi University, Nanning 530004, People's Republic of China
[13]Hangzhou Normal University, Hangzhou 310036, People's Republic of China
[14]Helmholtz Institute Mainz, Johann-Joachim-Becher-Weg 45, D-55099 Mainz, Germany
[15]Henan Normal University, Xinxiang 453007, People's Republic of China
[16]Henan University of Science and Technology, Luoyang 471003, People's Republic of China
[17]Huangshan College, Huangshan 245000, People's Republic of China
[18]Hunan University, Changsha 410082, People's Republic of China
[19]Indiana University, Bloomington, Indiana 47405, USA
[20a]INFN Laboratori Nazionali di Frascati, I-00044 Frascati, Italy
[20b]INFN and University of Perugia, I-06100 Perugia, Italy
[21a]INFN Sezione di Ferrara, I-44122 Ferrara, Italy
[21b]University of Ferrara, I-44122 Ferrara, Italy
[22]Institute of Physics and Technology, Peace Avenue 54B, Ulaanbaatar 13330, Mongolia
[23]Johannes Gutenberg University of Mainz, Johann-Joachim-Becher-Weg 45, D-55099 Mainz, Germany
[24]Joint Institute for Nuclear Research, 141980 Dubna, Moscow region, Russia
[25]Justus-Liebig-Universitaet Giessen, II. Physikalisches Institut,
Heinrich-Buff-Ring 16, D-35392 Giessen, Germany
[26]KVI-CART, University of Groningen, NL-9747 AA Groningen, Netherlands
[27]Lanzhou University, Lanzhou 730000, People's Republic of China
[28]Liaoning University, Shenyang 110036, People's Republic of China
[29]Nanjing Normal University, Nanjing 210023, People's Republic of China
[30]Nanjing University, Nanjing 210093, People's Republic of China
[31]Nankai University, Tianjin 300071, People's Republic of China
[32]Peking University, Beijing 100871, People's Republic of China
[33]Seoul National University, Seoul 151-747, Korea
[34]Shandong University, Jinan 250100, People's Republic of China
[35]Shanghai Jiao Tong University, Shanghai 200240, People's Republic of China
[36]Shanxi University, Taiyuan 030006, People's Republic of China
[37]Sichuan University, Chengdu 610064, People's Republic of China
[38]Soochow University, Suzhou 215006, People's Republic of China
[39]Southeast University, Nanjing 211100, People's Republic of China
[40]State Key Laboratory of Particle Detection and Electronics,
Beijing 100049, Hefei 230026, People's Republic of China
[41]Sun Yat-Sen University, Guangzhou 510275, People's Republic of China
[42]Tsinghua University, Beijing 100084, People's Republic of China
[43a]Ankara University, 06100 Tandogan, Ankara, Turkey
[43b]Istanbul Bilgi University, 34060 Eyup, Istanbul, Turkey
[43c]Uludag University, 16059 Bursa, Turkey
[43d]Near East University, Nicosia, North Cyprus, Mersin 10, Turkey
[44]University of Chinese Academy of Sciences, Beijing 100049, People's Republic of China
[45]University of Hawaii, Honolulu, Hawaii 96822, USA
[46]University of Jinan, Jinan 250022, People's Republic of China
[47]University of Minnesota, Minneapolis, Minnesota 55455, USA
[48]University of Muenster, Wilhelm-Klemm-Street 9, 48149 Muenster, Germany
[49]University of Science and Technology Liaoning, Anshan 114051, People's Republic of China

[50]University of Science and Technology of China, Hefei 230026, People's Republic of China
[51]University of South China, Hengyang 421001, People's Republic of China
[52]University of the Punjab, Lahore-54590, Pakistan
[53a]University of Turin, I-10125 Turin, Italy
[53b]University of Eastern Piedmont, I-15121 Alessandria, Italy
[53c]INFN, I-10125 Turin, Italy
[54]Uppsala University, Box 516, SE-75120 Uppsala, Sweden
[55]Wuhan University, Wuhan 430072, People's Republic of China
[56]Zhejiang University, Hangzhou 310027, People's Republic of China
[57]Zhengzhou University, Zhengzhou 450001, People's Republic of China

(Received 15 March 2018; published 31 May 2018)

The charm semileptonic decays $D^+ \to \eta e^+\nu_e$ and $D^+ \to \eta' e^+\nu_e$ are studied with a sample of $e^+e^-$ collision data corresponding to an integrated luminosity of 2.93 $\mathrm{fb}^{-1}$ collected at $\sqrt{s} = 3.773$ GeV with the BESIII detector. We measure the branching fractions for $D^+ \to \eta e^+\nu_e$ to be $(10.74 \pm 0.81 \pm 0.51) \times 10^{-4}$, and for $D^+ \to \eta' e^+\nu_e$ to be $(1.91 \pm 0.51 \pm 0.13) \times 10^{-4}$, where the uncertainties are statistical and systematic, respectively. In addition, we perform a measurement of the form factor in the decay $D^+ \to \eta e^+\nu_e$. All the results are consistent with those obtained by the CLEO-c experiment.

DOI: 10.1103/PhysRevD.97.092009

## I. INTRODUCTION

Charm semileptonic (SL) decays involve both the $c$-quark weak decay and the strong interaction. In the standard model, the Cabibbo-Kobayashi-Maskawa (CKM) matrix [1] describes the mixing among the quark flavors in the weak decay. The strong interaction effects in the hadronic current are parameterized by a form factor, which is numerically calculable with lattice quantum chromodynamics (LQCD). The differential decay rate for the charm SL decay $D^+ \to \eta e^+\nu_e$, neglecting the positron mass, is given by

$$\frac{\mathrm{d}\Gamma(D^+ \to \eta e^+\nu_e)}{\mathrm{d}q^2} = \frac{G_F^2|V_{cd}|^2}{24\pi^3}|\vec{p}_\eta|^3|f_+(q^2)|^2, \quad (1)$$

where $G_F$ is the Fermi constant, $V_{cd}$ is the relevant CKM matrix element, $\vec{p}_\eta$ is the momentum of the $\eta$ meson in the $D^+$ rest frame, and $f_+(q^2)$ is the form factor parametrizing the strong interaction dynamics as a function of the squared four-momentum transfer $q^2$, which is the square of the invariant mass of the $e^+$-$\nu_e$ pair. Precise measurements of the SL decay rates provide input to constrain the CKM matrix element $V_{cd}$ and to test the theoretical descriptions of the form factor. LQCD calculations of the form factor can be tested by comparing to the ones determined from the partial branching fraction (BF) measurements, once the CKM matrix element $V_{cd}$ is known.

The $\eta^{(\prime)}$ semileptonic modes are of special interest because they probe the mixing of $\eta$-$\eta'$ or $\eta$-$\eta'$-$G$, where $G$ represents a glueball. This mixing depends on many aspects of the underlying dynamics and hadronic structure of pseudoscalar mesons and glueballs [2] and could be important to theoretical calculations of the 2-body $D$ meson decays to a light pseudoscalar and vector or two pseudoscalars [3,4]. The existing measurements are based on light meson decays [5], $J/\psi$ decays [6], $B$ meson decays [7], and semileptonic decays of $D$ meson [2]. There is no confirmation of the gluonic components in $\eta^{(\prime)}$ meson up to date. The SL decays $D^+_{(s)} \to \eta^{(\prime)} e^+\nu_e$ can be used to study the $\eta$-$\eta'$ mixing in a much cleaner way than in hadronic processes due to the absence of final-state interaction [8]. Hence, measurements of the decays $D^+ \to \eta^{(\prime)} e^+\nu_e$ could add to our knowledge of the mixing of $\eta$ and $\eta'$.

Based on a data sample with an integrated luminosity of 818 $\mathrm{pb}^{-1}$ collected at $\sqrt{s} = 3.77$ GeV, the CLEO collaboration measured the BF for $D^+ \to \eta e^+\nu_e$ and $D^+ \to \eta' e^+\nu_e$ to be $\mathcal{B}_{\eta e^+\nu_e} = (11.4 \pm 0.9 \pm 0.4) \times 10^{-4}$

[a]Also at Bogazici University, 34342 Istanbul, Turkey.
[b]Also at the Moscow Institute of Physics and Technology, Moscow 141700, Russia.
[c]Also at the Functional Electronics Laboratory, Tomsk State University, Tomsk 634050, Russia.
[d]Also at the Novosibirsk State University, Novosibirsk 630090, Russia.
[e]Also at the NRC "Kurchatov Institute", PNPI, Gatchina 188300, Russia.
[f]Also at Istanbul Arel University, 34295 Istanbul, Turkey.
[g]Also at Goethe University Frankfurt, 60323 Frankfurt am Main, Germany.
[h]Also at Key Laboratory for Particle Physics, Astrophysics and Cosmology, Ministry of Education; Shanghai Key Laboratory for Particle Physics and Cosmology; Institute of Nuclear and Particle Physics, Shanghai 200240, People's Republic of China.
[i]Also at Government College Women University, Sialkot-51310. Punjab, Pakistan.
[j]Present address: Center for Underground Physics, Institute for Basic Science, Daejeon 34126, Korea.

and $\mathcal{B}_{\eta' e^+\nu_e} = (2.16 \pm 0.53 \pm 0.07) \times 10^{-4}$ [9], respectively. In this paper, we present new measurements of these BFs, using $D\bar{D}$ meson pairs produced near threshold at $\sqrt{s} = 3.773$ GeV with an integrated luminosity of 2.93 fb$^{-1}$ [10] collected with the BESIII detector [11]. In addition, the modulus of the form factor $f_+(q^2)$ in $D^+ \to \eta e^+\nu_e$ is measured.

## II. THE BESIII DETECTOR

The Beijing Spectrometer (BESIII) detects $e^+e^-$ collisions produced by the double-ring collider BEPCII. BESIII is a general-purpose detector [11] with 93% coverage of the full solid angle. From the interaction point (IP) to the outside, BESIII is equipped with a main drift chamber (MDC) consisting of 43 layers of drift cells, a time-of-flight (TOF) counter with double-layer scintillator in the barrel part and single-layer scintillator in the endcap section, an electromagnetic calorimeter (EMC) composed of 6240 CsI(Tl) crystals, a superconducting solenoid magnet providing a magnetic field of 1.0 T along the beam direction, and a muon counter containing multi-layer resistive plate chambers installed in the steel flux-return yoke of the magnet. The MDC spatial resolution is about 135 $\mu$m and the momentum resolution is about 0.5% for a charged track with transverse momentum of 1 GeV$/c$. The energy resolution for electromagnetic showers in the EMC is 2.5% at 1 GeV. More details of the spectrometer can be found in Ref. [11].

## III. MC SIMULATION

Monte Carlo (MC) simulation serves to estimate the detection efficiencies and to understand background components. High statistics MC samples are generated with a GEANT4-based [12] software package, which includes simulations of the geometry of the spectrometer and interactions of particles with the detector materials. KKMC is used to model the beam energy spread and the initial-state radiation (ISR) in the $e^+e^-$ annihilations [13]. The "inclusive" MC samples consist of the production of $D\bar{D}$ pairs with consideration of quantum coherence for all neutral $D$ modes, the non-$D\bar{D}$ decays of $\psi(3770)$, the ISR production of low mass $\psi$ states, and continuum processes (quantum electrodynamics (QED) and $q\bar{q}$). Known decays recorded by the Particle Data Group (PDG) [14] are simulated with EVTGEN [15] and the unknown decays with LUNDCHARM [16]. The final-state radiation (FSR) of charged tracks is taken into account with the PHOTOS package [17]. The equivalent luminosity of the inclusive MC samples is about 10 times that of the data. The signal processes of $D^+ \to \eta^{(\prime)} e^+\nu_e$ are generated using the modified pole model of Ref. [18].

## IV. DATA ANALYSIS

As the $\psi(3770)$ is close to the $D\bar{D}$ threshold, the pair of $D^+D^-$ mesons is produced nearly at rest without accompanying additional hadrons. Hence, it is straightforward to use the $D$-tagging method [19] to measure the absolute BFs, based on the following equation

$$\mathcal{B}_{\eta^{(\prime)} e^+\nu_e} = \frac{n_{\eta^{(\prime)} e^+\nu_e,\mathrm{tag}}}{n_{\mathrm{tag}}} \cdot \frac{\varepsilon_{\mathrm{tag}}}{\varepsilon_{\eta^{(\prime)} e^+\nu_e,\mathrm{tag}}}. \quad (2)$$

Here, $n_{\mathrm{tag}}$ is the total yield of the single-tag (ST) $D^-$ mesons reconstructed with hadronic decay modes, while $n_{\eta^{(\prime)} e^+\nu_e,\mathrm{tag}}$ is the number of the $D^+ \to \eta^{(\prime)} e^+\nu_e$ signal events when the ST $D^-$ meson is detected. $\varepsilon_{\mathrm{tag}}$ and $\varepsilon_{\eta^{(\prime)} e^+\nu_e,\mathrm{tag}}$ are the corresponding detection efficiencies. Note that in the context of this paper, charge conjugated modes are always implied.

### A. Reconstruction of the hadronic tag modes

The $D^-$ decay modes used for tagging are $K^+\pi^-\pi^-$, $K^+\pi^-\pi^-\pi^0$, $K_S^0\pi^-$, $K_S^0\pi^-\pi^0$, $K_S^0\pi^+\pi^-\pi^-$, and $K^+K^-\pi^-$, where $\pi^0 \to \gamma\gamma$ and $K_S^0 \to \pi^+\pi^-$. The sum of the BFs of these six decay modes is about 27.7%. $D^-$ tag candidates are reconstructed from all possible combinations of final state particles, according to the following selection criteria.

Momenta and impact parameters of charged tracks are measured by the MDC. Charged tracks are required to satisfy $|\cos\theta| < 0.93$, where $\theta$ is the polar angle with respect to the beam axis, and pass within $\pm 10$ cm of the interaction point along the beam axis and within $\pm 1$ cm in the plane perpendicular to the beam axis. Particle identification (PID) is implemented by combining the information of specific energy loss ($\mathrm{d}E/\mathrm{d}x$) in the MDC and the time of flight measurements from the TOF into PID likelihoods for the different particle hypotheses. For a charged $\pi(K)$ candidate, the likelihood of the $\pi(K)$ hypothesis is required to be larger than that of the $K(\pi)$ hypothesis.

Photons are reconstructed from energy deposition clusters in the EMC. The energies of photon candidates must be larger than 25 MeV for $|\cos\theta| < 0.8$ (barrel) and 50 MeV for $0.86 < |\cos\theta| < 0.92$ (end cap). To suppress fake photons due to electronic noise or beam backgrounds, the shower time must be less than 700 ns from the event start time [20].

The $\pi^0$ candidates are selected from pairs of photons of which at least one is reconstructed in the barrel. The two photon invariant mass, $M(\gamma\gamma)$, is required to lie in the range $(0.115, 0.150)$ GeV$/c^2$. We further constrain the invariant mass of each photon pair to the nominal $\pi^0$ mass, and update the four-momentum of the candidate according to the fit results.

The $K_S^0$ candidates are reconstructed via $K_S^0 \to \pi^+\pi^-$ using a vertex-constrained fit to all pairs of oppositely

TABLE I. Requirements on $\Delta E$, detection efficiencies and signal yields for the different ST modes. The errors are all statistical.

| Modes | $\Delta E$ (GeV) | $\epsilon_{\rm tag}$ (%) | $n_{\rm tag}$ |
|---|---|---|---|
| $K^+\pi^-\pi^-$ | $[-0.023, 0.022]$ | $50.94 \pm 0.03$ | $801283 \pm 949$ |
| $K^+\pi^-\pi^-\pi^0$ | $[-0.058, 0.032]$ | $25.40 \pm 0.03$ | $246770 \pm 699$ |
| $K_S^0\pi^-$ | $[-0.023, 0.024]$ | $52.59 \pm 0.09$ | $97765 \pm 328$ |
| $K_S^0\pi^-\pi^0$ | $[-0.064, 0.037]$ | $28.07 \pm 0.03$ | $217816 \pm 632$ |
| $K_S^0\pi^+\pi^-\pi^-$ | $[-0.027, 0.025]$ | $32.28 \pm 0.05$ | $126236 \pm 425$ |
| $K^+K^-\pi^-$ | $[-0.020, 0.019]$ | $40.08 \pm 0.08$ | $69869 \pm 326$ |

charged tracks, without PID requirements. The distance of closest approach of a charged track to the IP is required to be less than 20 cm along the beam direction, without requirement in the transverse plane. The $\chi^2$ of the vertex fit is required to be less than 100. The invariant mass of the $\pi^+\pi^-$ pair is required to lie in the range $(0.487, 0.511)$ GeV/$c^2$, which corresponds to three times the experimental mass resolution.

Two variables, the beam-constrained mass, $M_{\rm BC}$, and the energy difference, $\Delta E$, are used to identify the tagging signals, defined as follows

$$M_{\rm BC} \equiv \sqrt{E_{\rm beam}^2/c^4 - |\vec{p}_{D^-}|^2/c^2}, \quad (3)$$

$$\Delta E \equiv E_{D^-} - E_{\rm beam}. \quad (4)$$

Here, $\vec{p}_{D^-}$ and $E_{D^-}$ are the total momentum and energy of the $D^-$ candidate in the rest frame of the initial $e^+e^-$ system, and $E_{\rm beam}$ is the beam energy. Signals peak around the nominal $D^-$ mass in $M_{\rm BC}$ and around zero in $\Delta E$. Boundaries of $\Delta E$ requirements are set at $\pm 3\sigma$, except that those of modes containing a $\pi^0$ are set as $(-4\sigma, +3\sigma)$ due to the asymmetric distributions. Here, $\sigma$ is the standard deviation from the nominal value of $\Delta E$. In each event, only the combination with the least $|\Delta E|$ is kept for each $D^-$-tagging mode.

After applying the $\Delta E$ requirements in Table I in all the ST modes, we plot their $M_{\rm BC}$ distributions in Fig. 1. Maximum likelihood fits to these $M_{\rm BC}$ distributions are performed, in which the signals are modeled with the MC-simulated signal shape convolved with a smearing Gaussian function with free parameters, and the backgrounds are modeled with the ARGUS function [21]. The Gaussian functions are required in order to compensate for the resolution differences between data and MC simulations. Based on the fit results, ST yields of data are given in Table I in the $M_{\rm BC}$ mass range $[1.86, 1.88]$ GeV/$c^2$, along with their MC-determined detection efficiencies.

### B. Reconstruction of SL signals

We look for the SL signal of $D^+ \to \eta^{(\prime)} e^+ \nu_e$ in the events in which the ST $D^-$ mesons satisfy the requirement $1.86 \le M_{\rm BC} \le 1.88$ GeV/$c^2$. The positron and $\eta^{(\prime)}$ are reconstructed from the remaining tracks and neutral clusters that have not been used in the ST $D^-$ selection. Two $\eta$ decay modes $\eta \to \gamma\gamma$ (denoted as $\eta_{\gamma\gamma}$) and $\eta \to \pi^+\pi^-\pi^0$ (denoted as $\eta_{3\pi}$), and three $\eta'$ decay modes $\eta' \to \pi^+\pi^-\eta_{\gamma\gamma}$, $\eta' \to \pi^+\pi^-\eta_{3\pi}$ and $\eta' \to \gamma\rho^0 \to \gamma\pi^+\pi^-$, are studied. As the neutrino in the final states is undetectable at BESIII, the SL signals are identified by studying the variable $U_{\rm miss} = E_{\rm miss} - c|\vec{p}_{\rm miss}|$, where $E_{\rm miss} = E_{\rm beam} - E_{\eta^{(\prime)}} - E_{e^+}$ and $\vec{p}_{\rm miss} = \vec{p}_{D^+} - \vec{p}_{\eta^{(\prime)}} - \vec{p}_{e^+}$. $\vec{p}_{D^+}$ is the momentum of the $D^+$ meson, $E_{\eta^{(\prime)}}(\vec{p}_{\eta^{(\prime)}})$ and $E_{e^+}(\vec{p}_{e^+})$ are the energies (momenta) of the $\eta^{(\prime)}$ and $e^+$, respectively. The momentum $\vec{p}_{D^+}$ is calculated by $\vec{p}_{D^+} = -\hat{p}_{\rm tag}\sqrt{E_{\rm beam}^2/c^2 - m_{D^-}^2 c^2}$,

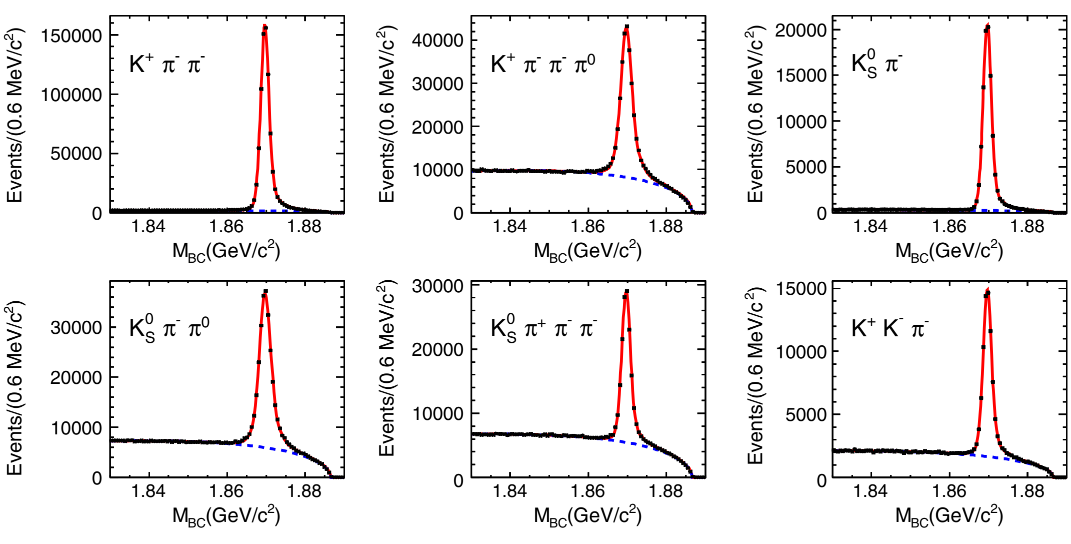


FIG. 1. Distributions of $M_{\rm BC}$ for the six ST modes. Data are shown as points with error bars. The solid lines are the total fits and the dashed lines are the background contribution.

where $\hat{p}_{\rm tag}$ is the momentum direction of the ST $D^-$ and $m_{D^-}$ is the nominal $D^-$ mass [14]. All the momenta are calculated in the rest frame of the initial $e^+e^-$ system. For the signal events, the $U_{\rm miss}$ distribution is expected to peak at zero.

Candidates for charged tracks, photons and $\pi^0$ are selected following the same selection criteria described above for the tagging $D^-$ hadronic modes. To select the $\eta \to \gamma\gamma$ candidates, the two-photon invariant mass is required to be within $(0.50, 0.58)$ GeV$/c^2$. A 1-C kinematic fit is performed to constrain this mass to the nominal $\eta$ mass, and the $\chi^2$ is required to be less than 20. If there are multiple $\eta \to \gamma\gamma$ candidates, only the one with the least $\chi^2$ is kept. The $\eta \to \pi^+\pi^-\pi^0$ candidates are required to have an invariant mass within $(0.52, 0.58)$ GeV$/c^2$. If multiple candidates exist per event, we only keep the candidate closest to the nominal $\eta$ mass. In the reconstruction of $D^+ \to \eta' e^+\nu_e$ signals, $\eta' \to \pi^+\pi^-\eta$ candidates are formed by combining an $\eta$ candidate with two charged pions. Their invariant mass must lie in $(0.935, 0.980)$ GeV$/c^2$ for $\eta' \to \pi^+\pi^-\eta_{2\gamma}$ and in $(0.930, 0.980)$ GeV$/c^2$ for $\eta' \to \pi^+\pi^-\eta_{3\pi}$; if multiple candidates are found, only the one closest to the nominal $\eta'$ mass is chosen. For $\eta' \to \gamma\rho^0$ candidate, we require a mass window $(0.55, 0.90)$ GeV$/c^2$ for $\rho^0 \to \pi^+\pi^-$ candidates, and the radiative photon is not to form a $\pi^0$ candidate with any other photon in the event. The energy of the radiative photon is required to be larger than 0.1 GeV in order to suppress $D^+ \to \rho^0 e^+\nu_e$ backgrounds. The helicity angle of the daughter pion in the rest frame of $\rho^0$, $\theta_{\pi\rho}$, is required to satisfy $|\cos\theta_{\pi\rho}| < 0.85$. To suppress backgrounds from FSR, the angle between the direction of the radiative photon and the positron momentum is required to be greater than 0.20 radians. Furthermore, the angles between the radiative photon and all charged tracks in the final state of the $D^-$ tag candidates are required to be larger than 0.52 radians, to suppress fake photons due to split-offs from hadronic showers in the EMC.

The positron is tracked in the MDC and distinguished from other charged particles by combining the $dE/dx$, TOF and EMC information. The determined PID likelihood $\mathcal{L}$ is required to satisfy $\mathcal{L}(e) > 0$ and $\mathcal{L}(e)/(\mathcal{L}(e)+\mathcal{L}(\pi)+\mathcal{L}(K)) > 0.8$. Furthermore, the energy measured in the EMC divided by the track momentum is required to be larger than 0.8 for $D^+ \to \eta e^+\nu_e$ and larger than 0.6 for $D^+ \to \eta' e^+\nu_e$. In addition, positron candidates with momentum less than 0.2 GeV$/c$ are discarded in $D^+ \to \eta' e^+\nu_e$ decays to reduce mis-PID rate. Events that have extra unused EMC showers with energies larger than 250 MeV, are discarded.

The resultant $U_{\rm miss}$ distributions are plotted in Fig. 2. We perform simultaneous unbinned maximum likelihood fits to the different decay modes for $\eta e^+\nu_e$ and $\eta' e^+\nu_e$, respectively. The signal shapes are obtained from MC simulations convolved with Gaussian functions whose widths are determined from the fit to account for the resolution difference in data and MC. Convolution with the Gaussians increases the overall width by approximately 15%. The background shapes of different $\eta^{(\prime)}$ decay modes are modeled with the distributions from backgrounds obtained from the inclusive MC sample. The uneven background shapes are caused by the fluctuations in the

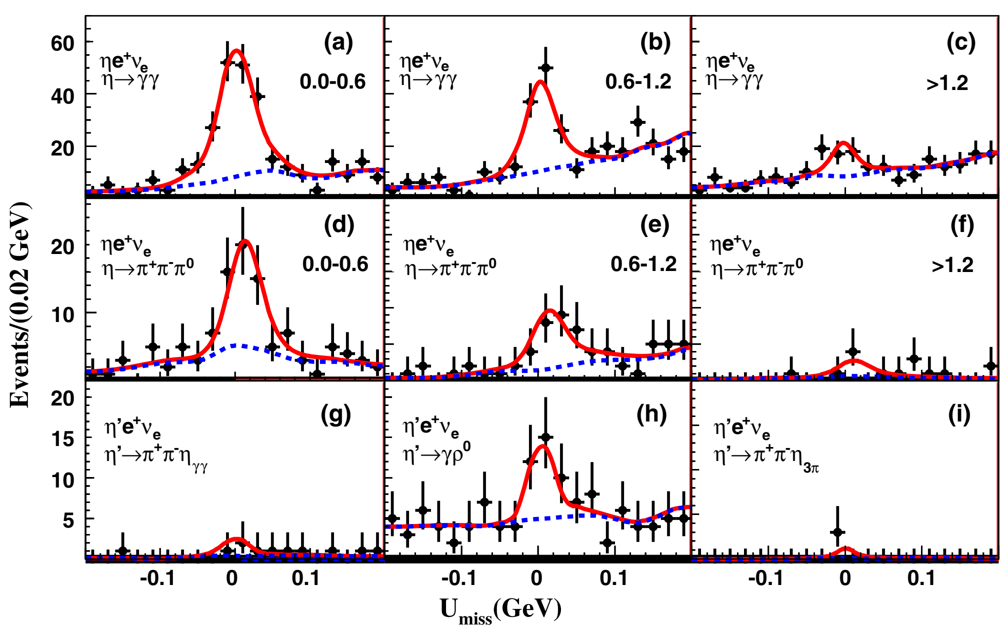


FIG. 2. Distributions of $U_{\rm miss}$ for the different signal modes. Data are shown as points with error bars. The solid lines are the total fits and the dashed lines are the background contributions. Data for $D^+ \to \eta e^+\nu_e$ are plotted in 3 bins of $0.0 \le q^2 < 0.6$ GeV$^2/c^4$ (a, d), $0.06 \le q^2 \le 1.2$ GeV$^2/c^4$ (b, e) and $q^2 > 1.2$ GeV$^2/c^4$ (c, f).

TABLE II. SL signal detection efficiencies for the different ST tag modes in percent. The errors are all statistical.

| Modes | $D^+ \to \eta e^+\nu_e$ | | $D^+ \to \eta' e^+\nu_e$ | | |
|---|---|---|---|---|---|
| Sub-decay modes | $\gamma\gamma$ | $\pi^+\pi^-\pi^0$ | $\pi^+\pi^-\eta_{\gamma\gamma}$ | $\pi^+\pi^-\eta_{3\pi}$ | $\gamma\rho^0$ |
| $K^+\pi^-\pi^-$ | $23.58 \pm 0.09$ | $12.65 \pm 0.07$ | $8.50 \pm 0.09$ | $2.41 \pm 0.05$ | $11.68 \pm 0.11$ |
| $K^+\pi^-\pi^-\pi^0$ | $9.77 \pm 0.07$ | $4.75 \pm 0.05$ | $3.48 \pm 0.06$ | $0.82 \pm 0.03$ | $4.96 \pm 0.07$ |
| $K^0_S\pi^-$ | $25.23 \pm 0.09$ | $13.45 \pm 0.08$ | $9.23 \pm 0.09$ | $2.29 \pm 0.05$ | $12.47 \pm 0.11$ |
| $K^0_S\pi^-\pi^0$ | $9.82 \pm 0.07$ | $5.40 \pm 0.05$ | $4.60 \pm 0.07$ | $0.83 \pm 0.03$ | $5.83 \pm 0.08$ |
| $K^0_S\pi^+\pi^-\pi^-$ | $13.98 \pm 0.08$ | $6.24 \pm 0.05$ | $4.09 \pm 0.06$ | $0.82 \pm 0.03$ | $5.87 \pm 0.08$ |
| $K^+K^-\pi^-$ | $18.41 \pm 0.09$ | $9.93 \pm 0.07$ | $6.28 \pm 0.08$ | $1.52 \pm 0.04$ | $8.18 \pm 0.09$ |

inclusive MC sample. In total, we observe $373 \pm 26$ signal events for $D^+ \to \eta e^+\nu_e$ and $31.6 \pm 8.4$ for $D^+ \to \eta' e^+\nu_e$. The BF for $D^+ \to \eta^{(\prime)} e^+\nu_e$ is determined by using Eq. (2) according to the MC-determined efficiencies in Table II, which gives $\mathcal{B}_{\eta e^+\nu_e} = (10.74 \pm 0.81) \times 10^{-4}$, and $\mathcal{B}_{\eta' e^+\nu_e} = (1.91 \pm 0.51) \times 10^{-4}$.

The yield of $D^+ \to \eta e^+\nu_e$ candidates is sufficient to determine $|f_+(q^2)|$, as defined in Eq. (1). Hence, a fit is implemented to the partial BFs in the three $q^2$ bins used in Fig. 2. By introducing the life time $\tau_{D^+} = (1040 \pm 7) \times 10^{-15}$ s from PDG [14], we construct $\chi^2 = \Delta\gamma^T V^{-1} \Delta\gamma$, where $\Delta\gamma = \Delta\Gamma_m - \Delta\Gamma_p$ is the vector of differences between the measured partial decay widths $\Delta\Gamma_m$ and the expected partial widths $\Delta\Gamma_p$ integrated over the different $q^2$ bins, and $V$ is the total covariance matrix consisting of the statistical covariance matrix $V_{\rm stat}$ and the systematic covariance $V_{\rm syst}$. The statistical correlations among the different $q^2$ bins are negligible. We list the elements of the total covariance matrix $V$ in Table III.

Three parametrizations of the form factor $f_+(q^2)$ are adopted in the fits. The first form is the simple pole model of Ref. [18], which is given by

$$f_+(q^2) = \frac{f_+(0)}{1 - \frac{q^2}{m^2_{\rm pole}}}. \tag{5}$$

Here, $m_{\rm pole}$ is predicted to be close to the mass of $D^{*+}$ [14], which is 2.01 GeV$/c^2$ and is a free parameter in the fit. The second choice is the modified pole model [18], written as

$$f_+(q^2) = \frac{f_+(0)}{\left(1 - \frac{q^2}{m^2_{\rm pole}}\right)\left(1 - \alpha\frac{q^2}{m^2_{\rm pole}}\right)}, \tag{6}$$

TABLE III. Correlation matrix including statistical and systematic contributions in the fit.

| $q^2$(GeV$^2$/c$^4$) | 0.0–0.6 | 0.6–1.2 | >1.2 |
|---|---|---|---|
| 0.0–0.6 | 1 | 0.075 | 0.032 |
| 0.6–1.2 | 0.075 | 1 | 0.026 |
| >1.2 | 0.032 | 0.026 | 1 |

where $m_{\rm pole}$ is fixed at the mass of $D^{*+}$ and $\alpha$ is a free parameter to be determined. The third is a general series parametrization with $z$-expansion, which is formulated as

$$f_+(q^2) = \frac{1}{P(q^2)\phi(q^2, t_0)} \sum_{k=0}^{\infty} a_k(t_0)[z(q^2, t_0)]^k. \tag{7}$$

Here, $t_0 = t_+(1 - \sqrt{1 - t_-/t_+})$ with $t_\pm = (m_{D^+} \pm m_\eta)^2$ and $a_k(t_0)$ are real coefficients. The functions $P(q^2)$, $\phi(q^2, t_0)$ and $z(q^2, t_0)$ are formulated following the definitions in Ref. [22]. In the fit, the series is truncated at $k = 1$.

Three separate fits to data are implemented, based on the three form-factor models. Their fit curves are plotted in Fig. 3. We determine the values of $f_+(0)|V_{cd}|$ in all three scenarios, as listed in Table IV. We observe that the results of $f_+(0)|V_{cd}|$ in the three fits are consistent and the fit qualities are good.

## V. SYSTEMATIC UNCERTAINTIES

With the double-tag technique, the systematic uncertainties in the detection efficiency of the ST $D^-$ mesons in the

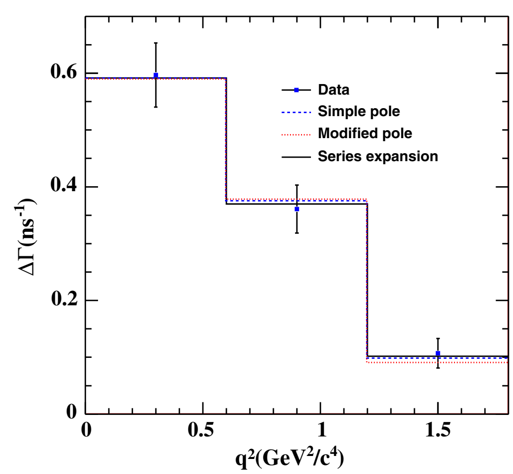


FIG. 3. Fit to the partial widths of $D^+ \to \eta e^+\nu_e$. The dots with error bars are data and the lines are the fits with different form-factor models.

TABLE IV. The fit results of the form-factor parameters. For simple pole and modified pole parametrizations, shape parameters denote $m_{\rm pole}$ and $\alpha$, respectively. For the series parametrization, the shape parameter is $r_1 = a_1/a_0$. The correlation coefficients $\rho$ between fitting parameters and the reduced $\chi^2$ are given.

| Fit parameters | Simple pole | Modified pole | Series expansion |
|---|---|---|---|
| $f_+(0)\lvert V_{cd}\rvert$ ($\times 10^{-2}$) | $8.15 \pm 0.45 \pm 0.18$ | $8.24 \pm 0.51 \pm 0.22$ | $7.86 \pm 0.64 \pm 0.21$ |
| Shape parameter | $1.73 \pm 0.17 \pm 0.03$ | $0.50 \pm 0.54 \pm 0.08$ | $-7.33 \pm 1.69 \pm 0.40$ |
| $\rho$ | 0.80 | $-0.85$ | 0.90 |
| $\chi^2$/ndf | $0.1/(3-2)$ | $0.3/(3-2)$ | $0.5/(3-2)$ |

BF measurements mostly cancel as shown in Eq. (2). For the SL signal side, the following sources of systematic uncertainties are studied, as summarized in Table V. All of these contributions are added in quadrature to obtain the total systematic uncertainties in the BFs.

The uncertainties in tracking and PID efficiencies for $\pi^\pm$ are studied with control samples of $D\bar{D}$ Cabibbo favored ST decays [23]. The uncertainties in $e^\pm$ tracking and PID efficiencies are estimated with radiative Bhabha events, taking account of the dependence of the $e^{pm}$ tracking and PID efficiencies on $\cos\theta$ and momentum.

The uncertainty due to $\pi^0$ and $\eta$ reconstruction efficiencies is estimated with a control sample using $D^0 \to K^-\pi^+\pi^0$ selected without requiring the $\pi^0$ meson. The uncertainties associated with the $\eta$ and $\eta'$ invariant mass requirements are estimated by changing the requirement boundaries and taking the maximum variations of the resultant BFs as systematic uncertainties. The uncertainty due to the extra shower veto is studied with doubly tagged hadronic events, and is found to be negligible.

The uncertainties of the radiative $\gamma$ selection in $\eta' \to \gamma\rho^0$ are studied using a control sample from $D^0\bar{D}^0$ decays where the $D^0$ meson decays to $K_S^0\eta'$, $\eta' \to \gamma\rho^0$ and the $\bar{D}^0$ decays to Cabibbo favored ST modes. We impose the same selection criteria on the radiative photon in the control sample, and find that the difference between the signal survival rates in data and MC simulation is 3.1%. The uncertainty due to the $\rho$ invariant mass requirement is also estimated with this control sample. The difference of signal survival rates between data and MC simulations is found to be 0.6%.

In the fit to the $U_{\rm miss}$ distribution, the uncertainty due to the parametrization of the signal shape is estimated by introducing a Gaussian function to smear the MC-simulated signal shape and varying the parameters of the smearing Gaussian. The uncertainty due to the background modeling is estimated by changing the background model to a 3rd degree Chebychev polynomial. The uncertainty due to the fit range is estimated by repeating the fits in several different ranges. The uncertainties in the input BFs and arising from the limited MC statistics are also taken into account.

We also study the $\Delta E$ and $M_{\rm BC}$ requirements by varying the ranges and compare the efficiency-corrected tag yields. The resultant maximum differences are taken as systematic uncertainties. The SL signal model for $D^+ \to \eta e^+\nu_e$ is simulated according to the form factor measured in this work and the variations within one standard deviation are studied. For $D^+ \to \eta' e^+\nu_e$, since there is no available form-factor data, we take the form factor of $D^+ \to \eta e^+\nu_e$ and evaluate the systematic uncertainty as we do for $D^+ \to \eta e^+\nu_e$.

Systematic uncertainties in the partial decay widths of $D^+ \to \eta e^+\nu_e$ to calculate the correlation matrix $V_{\rm syst}$. are studied following the same procedure mentioned above. For most of the common systematics, we quote the values from the total BF measurements in Table V. For charged pion tracking and PID, we evaluate the uncertainty averaged over the two $\eta$ decay modes according to their relative yields. For $e^+$ tracking and PID, we reweight the systematic uncertainties in each $q^2$ bin. All these items are summarized in Table VI. For the uncertainties associated with the $\eta$ mass window and fitting procedure, we refit the $U_{\rm miss}$ distribution after varying the $\eta$ mass window and changing fitting region and compare the refitting results of the form factors. The maximum deviations from the nominal results are calculated to be 1.3% and 0.4% for the $f_+(0)|V_{cd}|$ and shape parameter and are incorporated into the systematic uncertainties. The sum of the systematic uncertainties is given in Table IV.

TABLE V. Relative systematic uncertainties in the BF measurements (in %). The lower half of the table presents the common uncertainties among the different channels.

| Source | $D^+ \to \eta e^+\nu_e$ | | $D^+ \to \eta' e^+\nu_e$ | | |
|---|---|---|---|---|---|
| Subdecay modes | $\gamma\gamma$ | $\pi^+\pi^-\pi^0$ | $\pi^+\pi^-\eta_{\gamma\gamma}$ | $\pi^+\pi^-\eta_{3\pi}$ | $\gamma\rho$ |
| $\pi^\pm$ tracking and PID | | 2.8 | 4.1 | 8.2 | 1.6 |
| $\pi^0/\eta$ reconstruction | 2.0 | 2.0 | 2.2 | 2.2 | |
| Input BF | 0.3 | 0.3 | 1.7 | 2.0 | 1.7 |
| $\rho$ mass window | | | | | 0.6 |
| Radiative $\gamma$ | | | | | 3.1 |
| $\eta'$ mass window | | | 1.8 | 1.6 | 1.9 |
| $e^+$ tracking and PID | 1.1 | | 3.7 | | |
| $\eta$ mass window | 2.4 | | 2.4 | | |
| $U_{\rm miss}$ fit | 2.1 | | 1.0 | | |
| $\Delta E/M_{\rm BC}$ window | 0.9 | | 0.9 | | |
| MC statistics | 0.2 | | 0.5 | | |
| SL signal model | 0.9 | | 0.9 | | |
| Total | 4.7 | | 6.9 | | |

TABLE VI. Relative systematic uncertainties (in %) of the measured partial decay widths of $D^+ \to \eta e^+ \nu_e$ used to obtain $V_{\rm syst}$.

| | $q^2(\mathrm{GeV}^2/\mathrm{c}^4)$ | | |
|---|---|---|---|
| Source | 0.0–0.6 | 0.6–1.2 | >1.2 |
| $e^+$ tracking and PID | 1.4 | 0.9 | 0.1 |
| $\pi^\pm$ tracking and PID | 1.7 | | |
| $\pi^0/\eta$ reconstruction | 2.0 | | |
| $\Delta E/M_{\rm BC}$ window | 0.9 | | |
| MC statistics | 0.2 | | |
| SL signal model | 0.9 | | |
| Input BF | 0.3 | | |
| $D^+$ lifetime | 0.7 | | |
| Total | 3.3 | 3.0 | 2.9 |

## VI. SUMMARY

We exploit a double-tag technique to analyze a sample of 2.93 fb$^{-1}$ $e^+e^- \to D^+D^-$ at $\sqrt{s} = 3.773$ GeV. The BF for the SL decay $D^+ \to \eta e^+\nu_e$ is measured to be $\mathcal{B}_{\eta e^+\nu_e} = (10.74 \pm 0.81 \pm 0.51) \times 10^{-4}$, and for $D^+ \to \eta' e^+\nu_e$ to be $\mathcal{B}_{\eta' e^+\nu_e} = (1.91 \pm 0.51 \pm 0.13) \times 10^{-4}$, where the first and second uncertainties are statistical and systematic, respectively. In addition, we measure the decay form factor for $D^+ \to \eta e^+\nu_e$ based on three form-factor models, whose results are given in Table IV. This helps to calibrate the form-factor calculation in LQCD. All these results are consistent with the previous measurements from CLEO-c [9]. Our precision is only slightly better than CLEO-c's, because our limitations on PID and low-momentum tracking efficiency hinder the adoption of CLEO-c's generic $D$-tagging method [9]. The average values of the CLEO-c results and ours for $\mathcal{B}_{\eta e^+\nu_e}$ and $\mathcal{B}_{\eta' e^+\nu_e}$ are $(11.04 \pm 0.60 \pm 0.33) \times 10^{-4}$ and $(2.04 \pm 0.37 \pm 0.08) \times 10^{-4}$, respectively. Using the input value recommended by Ref. [2], the $\eta$-$\eta'$ mixing angle $\phi_P$ is determined to be $(40 \pm 3 \pm 3)^\circ$, where the first uncertainty is experimental and the second theoretical, and in agreement with the results obtained by Refs. [2,5–7]. However, the current precision for $D^+ \to \eta^{(\prime)} e^+\nu_e$ is not enough to provide meaningful constraints on the $\eta$-$\eta'$ mixing parameters.

## ACKNOWLEDGMENTS

The BESIII collaboration thanks the staff of BEPCII, the IHEP computing center and the supercomputing center of USTC for their strong support. This work is supported in part by National Key Basic Research Program of China under Contract No. 2015CB856700; National Natural Science Foundation of China (NSFC) under Contracts No. 11605198, No. 11335008, No. 11375170, No. 11425524, No. 11475164, No. 11475169, No. 11605196, No. 11625523, No. 11635010, No. 11735014; the Chinese Academy of Sciences (CAS) Large-Scale Scientific Facility Program; the CAS Center for Excellence in Particle Physics (CCEPP); Joint Large-Scale Scientific Facility Funds of the NSFC and CAS under Contracts No. U1532102, No. U1532257, No. U1532258, No. U1732263; CAS Key Research Program of Frontier Sciences under Contracts No. QYZDJ-SSW-SLH003, No. QYZDJ-SSW-SLH040; 100 Talents Program of CAS; INPAC and Shanghai Key Laboratory for Particle Physics and Cosmology; German Research Foundation DFG under Contracts Nos. Collaborative Research Center CRC 1044, FOR 2359; Istituto Nazionale di Fisica Nucleare, Italy; Koninklijke Nederlandse Akademie van Wetenschappen (KNAW) under Contract No. 530-4CDP03; Ministry of Development of Turkey under Contract No. DPT2006K-120470; National Science and Technology fund; The Swedish Research Council; U.S. Department of Energy under Contracts No. DE-FG02-05ER41374, No. DE-SC-0010118, No. DE-SC-0010504, No. DE-SC-0012069; University of Groningen (RuG) and the Helmholtzzentrum fuer Schwerionenforschung GmbH (GSI), Darmstadt.

[1] N. Cabibbo, Phys. Rev. Lett. **10**, 531 (1963); M. Kobayashi and T. Maskawa, Prog. Theor. Phys. **49**, 652 (1973).
[2] H. W. Ke, X. Q. Li, and Z. T. Wei, Eur. Phys. J. C **69**, 133 (2010); H. Li, Nucl. Phys. B, Proc. Suppl. **162**, 312 (2006).
[3] B. Bhattacharya and J. L. Rosner, Phys. Rev. D **82**, 037502 (2010).
[4] B. Bhattacharya and J. L. Rosner, Phys. Rev. D **81**, 014026 (2010).
[5] F. Ambrosino *et al.*, J. High Energy Phys. 07 (2009) 105.
[6] R. Escribano, Eur. Phys. J. C **65**, 467 (2010).
[7] R. Aaij *et al.* (LHCb Collaboration), J. High Energy Phys. 01 (2015) 024.
[8] C. Di Donato, G. Ricciardi, and I. I. Bigi, Phys. Rev. D **85**, 013016 (2012).
[9] J. Yelton *et al.* (CLEO Collaboration), Phys. Rev. D **84**, 032001 (2011).
[10] M. Ablikim *et al.* (BESIII Collaboration), Chin. Phys. C **37**, 123001 (2013); M. Ablikim *et al.* (BESIII Collaboration), Phys. Lett. B **753**, 629 (2016).
[11] M. Ablikim *et al.* (BESIII Collaboration), Nucl. Instrum. Methods Phys. Res, Sect. A **614**, 345 (2010).
[12] S. Agostinelli *et al.* (GEANT4 Collaboration), Nucl. Instrum. Methods Phys. Res., Sect. A **506**, 250 (2003).

[13] S. Jadach, B. F. L. Ward, and Z. Was, Phys. Rev. D **63**, 113009 (2001).
[14] C. Patrignani *et al.* (Particle Data Group), Chin. Phys. C **40**, 100001 (2016).
[15]` D. J. Lange, Nucl. Instrum. Methods Phys. Res., Sect. A **462**, 152 (2001); P. Rong-Gang, Chin. Phys. C **32**, 599 (2008).
[16] J. C. Chen, G. S. Huang, X. R. Qi, D. H. Zhang, and Y. S. Zhu, Phys. Rev. D **62**, 034003 (2000).
[17] E. Richter-Was, Phys. Lett. B **303**, 163 (1993).
[18] D. Becirevic and A. B. Kaidalov, Phys. Lett. B **478**, 417 (2000).
[19] R. M. Baltrusaitis *et al.* (MARK-III Collaboration), Phys. Rev. Lett. **56**, 2140 (1986); J. Adler *et al.* (MARK-III Collaboration), Phys. Rev. Lett. **60**, 89 (1988).
[20] X. Ma *et al.*, Chin. Phys. C **32**, 744 (2008); Y. Guan, X.-R. Lu, Y. Zheng, and Y.-F. Wang, Chin. Phys. C **38**, 016201 (2014).
[21] H. Albrecht *et al.* (ARGUS Collaboration), Phys. Lett. B **241**, 278 (1990).
[22] T. Becher and R. J. Hill, Phys. Lett. B **633**, 61 (2006).
[23] M. Ablikim *et al.* (BESIII Collaboration), Phys. Rev. D **92**, 072012 (2015).